Analogs for Earth-Moon Halo Orbits and their Evolving Characteristics in Higher-Fidelity Force Models

Kenza K. Boudad* and Kathleen C. Howell†
Purdue University, West Lafayette, IN, 47907

Diane C. Davis ‡
a.i.solutions, Inc., Houston, TX 77058

Quasi-periodic or bounded motion in the ephemeris model is generally constructed by transitioning a solution from a lower-fidelity model, such as the Circular Restricted Three-Body Problem (CR3BP). Increased interest in the Earth-Moon L_2 Near Rectilinear Halo Orbits (NRHOs) within the context of the upcoming Gateway program supports the need for reliable transition methods for trajectories to the ephemeris force model. However, the characteristics of certain NRHOs, such as the 3:1 synodic resonant NRHO, are not maintained in the ephemeris model when directly transitioned from the Earth-Moon CR3BP with the current methodology. This investigation proposes a transition method that employs the Earth-Moon-Sun Bicircular Restricted Four-Body Problem (BCR4BP) as an intermediate step to address some the challenges associated with the direct transition method. By incorporating additional perturbations in the intermediate step, the quality of the initial guesses for the quasi-periodic orbit in the ephemeris model is increased. Consequently, the desired characteristics and geometry of the lower-fidelity solutions are further maintained along the trajectories obtained in the ephemeris model.

I. Introduction

As evidenced by the Global Exploration Roadmap [1], international interest exists in a new era of human exploration of the solar system. Such an effort is commencing investigations for maintaining a facility—at times crewed—in a orbit near the Moon. The proposed Gateway [2] concept is the current framework for the NASA development of this space facility. From a baseline trajectory in a Near Rectilinear Halo Orbit (NRHO), the Gateway is intended to serve as a proving ground for deep space technologies and as a staging location for missions beyond low Earth orbit. While the NRHOs are identified in cislunar space in terms of the Earth-Moon Circular Restricted Three-Body Problem (CR3BP), the impact of solar gravity and various other perturbations may at times be significant. Thus, it is increasingly important that different dynamical models are leveraged at different steps in the trajectory design process. In this investigation, three dynamical models are employed to construct representative members of the Earth-Moon halo family of periodic orbits and one of its subsets, the NRHOs. The Circular Restricted Three-Body Problem (CR3BP) [3] is an autonomous model approximating the Earth-Moon dynamics. The Bicircular Restricted Four-Body Problem [4] is a time-dependent, periodic model describing the motion of a spacecraft in the Earth-Moon-Sun regime. The BCR4BP can serve as an intermediate step between the CR3BP and a high-fidelity, time-dependent, non-periodic ephemeris model. This ephemeris model leverages the N-body differential equations and provides a higher-fidelity framework for analysis and verification of results produced in the CR3BP and the BCR4BP. The ephemeris model also captures additional forces that must be accommodated in actual flight.

Stacking revolutions of a periodic orbit in a lower-fidelity model and employing a differential corrections scheme is an effective strategy to construct bounded motions or quasi-periodic orbits in the ephemeris model and produces useful analogs that frequently preserve the characteristics deemed important for the application. A direct transition from the lower- to the higher-fidelity model is sufficient in many cases to maintain the desired characteristics and geometry of the solution throughout the transition. However, it is not effective for certain periodic orbits from the Earth-Moon CR3BP, such as the L_2 3:1 synodic resonant NRHO. When directly transitioned from the CR3BP, the resulting solution in the ephemeris results in either a 'tightly' or 'loosely' converged geometry; neither type of solution resembles the periodic orbit in the CR3BP. While the orbital and stability characteristics of the 3:1 NRHO in the CR3BP do not set it

*PhD Candidate, School of Aeronautics and Astronautics, Purdue University, kboudad@purdue, AIAA Student Member.
†Hsu Lo Distinguished Professor of Aeronautics and Astronautics, School of Aeronautics and Astronautics, Purdue University, AIAA Fellow.
‡Principal Systems Engineer, a.i. solutions, Inc., 2224 Bay Area Blvd, Houston, TX 77058, AIAA Associate Fellow.

apart from the other orbits in the L_2 halo family of periodic orbits, it does exist in a complex dynamical environment. Multiple bifurcations to other families of periodic orbit exist in the near vicinity of the 3:1 NRHO. Transitioning the 3:1 NRHO directly from the CR3BP to the ephemeris model is not an effective approach to obtain bounded, repeatable motion in the higher-fidelity model.

This investigation proposes a method that employs a second lower-fidelity dynamical model, the Earth-Moon-Sun BCR4BP, as an intermediate step in the transition process from the Earth-Moon CR3BP to the higher-fidelity ephemeris model. By incorporating additional perturbations in the intermediate step, the quality of the initial guess for the quasi-periodic orbit for the ephemeris model is increased. Consequently, the desired characteristics of the motion are further maintained along the solutions in the ephemeris model. The effectiveness of the proposed strategy is verified with the transition of the 3:1 synodic resonant NRHO to the ephemeris model. Additionally, various metrics are defined to quantify the quality of the transition process, rather than relying solely on visual inspection.

II. Background

A. Dynamical Models

Three dynamical models are employed in this investigation. The Circular Restricted 3-Body Problem (CR3BP) [3] is an autonomous model approximating the Earth-Moon system dynamics. The Bicircular Restricted 4-Body Problem (BCR4BP) [5] is a time-dependent, periodic model describing the motion of a particle in the Earth-Moon-Sun regime. Finally, an N-body model based on ephemeris data provides higher-fidelity analysis for particular mission scenarios.

The Circular Restricted 3-Body Problem

In the CR3BP, the motion of a spacecraft of negligible mass is subject to the influence of two primary gravitational bodies, for example, the Earth and the Moon. The model assumes that the two primaries are point masses in circular orbits about their common center of mass. The motion of the spacecraft under the influence of the two primaries is described relative to a rotating frame moving at a fixed rate consistent with the circular rotation of the primaries. By convention, the differential equations governing the CR3BP are nondimensionalized. The characteristic quantities employed include: (i) the Earth-Moon distance; (ii) the sum of the primary masses; (iii) a characteristic time such that the nondimensional gravitational constant $\tilde{G}$ equals unity. The nondimensional equations of motion are then

$$\ddot{x} = 2\dot{y} + \frac{\partial U^*}{\partial x}, \quad \ddot{y} = -2\dot{x} + \frac{\partial U^*}{\partial y}, \quad \ddot{z} = \frac{\partial U^*}{\partial z} \tag{1}$$

where x, y, z (respectively, $\dot{x}, \dot{y}, \dot{z}$) are the position (respectively, the velocity) components of the spacecraft expressed in the Earth-Moon rotating coordinates and derivatives as viewed by an observer in the rotating frame. The associated pseudo-potential function U^* is defined as

$$U^* = \frac{1}{2}(x^2 + y^2) + \frac{\mu}{r_{\text{e-sc}}} + \frac{1-\mu}{r_{\text{m-sc}}} \tag{2}$$

The quantities $r_{\text{e-sc}}$ and $r_{\text{m-sc}}$ are the distances between the spacecraft and the primaries, and $\mu = {m_{\text{m}}}/{(m_{\text{e}}+m_{\text{m}})}$ is the mass parameter for the Earth-Moon CR3BP system.

The equations of motion in the CR3BP do not admit a closed-form solution. However, five equilibrium solutions, the libration points, exist and are denoted L_1 through L_5. Stable and unstable orbits in families, such as the L_2 halo orbit family, exist in the CR3BP. The CR3BP allows a single integral of the motion, the Jacobi constant, evaluated as

$$C = 2U^* - \left(\dot{x}^2 + \dot{y}^2 + \dot{z}^2\right) \tag{3}$$

This energy-like quantity limits the motion of the spacecraft to regions where the magnitude of the rotating velocity is real and not a complex quantity. These regions are bounded by Zero Velocity Surfaces (ZVSs). For values of the Jacobi constant greater than the one associated with the L_1 libration point, the ZVSs form two closed regions around each of the primaries. As the energy along the spacecraft trajectory increases, the value of the Jacobi constant decreases until, at the L_1 value, the ZVSs open at the L_1 libration point, and the spacecraft is able to move from the vicinity of one primary to the vicinity of the other. Similarly, when the value of the Jacobi constant decreases to the value associated with L_2, the ZVSs open at L_2 allowing escape beyond the vicinity of the primaries entirely. Thus, the Jacobi constant is an energy-like quantity that bounds motion in the CR3BP.

The Bicircular Restricted 4-Body Problem

In scenarios where the gravitational influence of the Sun is non-negligible, a higher-fidelity model is necessary to accurately describe the spacecraft behavior. The BCR4BP incorporates the gravitational effect of three massive bodies, for instance, the Earth, the Moon and the Sun, on the motion of a spacecraft [5–7]. The mass of the spacecraft is assumed to be negligible in comparison to the masses of the other bodies. In this model, the Earth and the Moon are assumed to move in circular orbits around their common barycenter, denoted B_1, while the Sun and B_1 move in circular orbits with respect to the Earth-Moon-Sun barycenter, labeled B_2, as denoted in Fig. 1(b). The BCR4BP is not a coherent model: the perturbing acceleration from the Sun does not influence the motion of the Earth and the Moon, thus, the motion of the Moon is not a solution to the Sun-Earth CR3BP. Coherent bicircular models have been investigated previously [6], but are not necessary in this analysis. The equations of motion in the CR3BP, in Eq. (1), are extended to include the solar gravitational influence as follows,

$$\ddot{x} \;\; = 2\dot{y} + \frac{\partial \Upsilon^*}{\partial x}, \quad \ddot{y} \;\; = -2\dot{x} + \frac{\partial \Upsilon^*}{\partial y}, \quad \ddot{z} \;\; = \frac{\partial \Upsilon^*}{\partial z} \tag{4}$$

where Υ^* is the pseudo-potential function in the BCR4BP and evaluated as

$$\Upsilon^* = U^* + \frac{\mu_\mathrm{s}}{r_\mathrm{s\text{-}sc}} - \frac{\mu_\mathrm{s}}{a_\mathrm{s}^3}(x_\mathrm{s}x + y_\mathrm{s}y + z_\mathrm{s}z) \tag{5}$$

Then, $\mu_\mathrm{s} = \frac{m_\mathrm{s}}{m_\mathrm{e}+m_\mathrm{m}}$ is the nondimensional mass of the Sun and $a_\mathrm{s} = \frac{r_\mathrm{s}}{r_\mathrm{e\text{-}m}}$ is the nondimensional distance between the Earth-Moon barycenter and the Sun. Note that this adaptation of the BCR4BP assumes the Sun moves in the Earth-Moon plane of motion. The Earth-Moon and Sun-B_1 systems can be modeled in different planes[7], but a planar model suffices for this application. The variables $x_\mathrm{s}, y_\mathrm{s}, z_\mathrm{s}$ are the position components of the Sun, originating at B_1, and expressed in terms of the Earth-Moon rotating frame,

$$\begin{bmatrix} x_\mathrm{s} \\ y_\mathrm{s} \\ z_\mathrm{s} \end{bmatrix} = a_\mathrm{s} \begin{bmatrix} \cos(\theta) \\ \sin(\theta) \\ 0 \end{bmatrix} = \begin{bmatrix} \cos(-\omega\, t + \theta_0) \\ \sin(-\omega\, t + \theta_0) \\ 0 \end{bmatrix} \tag{6}$$

where the Sun angle θ is measured from the rotating $\hat{x}$ axis to the Sun position vector as defined in Fig. 1(a), and $\omega = 0.9253$ is the magnitude of the nondimensional angular velocity of the Sun as viewed in the Earth-Moon rotating frame[5]. This angular velocity is computed as the difference between the nondimensional mean motion of the Sun in the inertial frame centered at the Earth-Moon barycenter, that is, $n_S = \sqrt{(1+\mu_\mathrm{s})/a_\mathrm{s}^3}$, and the nondimensional mean motion of the Earth-Moon system with respect to the same observer, n, that is, the value one. Observe that the independent time variable, t, explicitly appears in the BCR4BP pseudo-potential through the Sun terms. Therefore, the BCR4BP is time-dependent and does not admit an integral of the motion. However, a scaled version of the Hamiltonian value in the BCR4BP is defined to be consistent with the Jacobi constant in the CR3BP, i.e.,

$$H(\theta) = 2\Upsilon^* - \left(\dot{x}^2 + \dot{y}^2 + \dot{z}^2\right) \tag{7}$$

Note that the Hamiltonian value is a function of the Sun angle θ and, thus, a function of the independent time variable. Equation (7) relates nondimensional position and velocity states. Thus, similar to the Jacobi constant in the CR3BP, the Hamiltonian, is a nondimensional metric. Equations (4) to (7) describe the Earth-Moon-Sun BCR4BP as defined in the Earth-Moon rotating frame.

The N-Body Ephemeris Model

For applications in mission scenarios where high-fidelity modeling accuracy is required, the N-Body differential equations and planetary ephemerides are employed. The N-body dynamics describe the motion of a particle of interest (e.g., a spacecraft), labeled P_i, subject to the gravitational influence of a central body, P_c, and N perturbing bodies $P_1, P_2, \ldots, P_\mathrm{N}$, all assumed to be modeled as particles. The position state vector, $\bar{\rho}$, for each of the bodies is expressed in inertial coordinates relative to the central body P_c, as denoted in Fig. 1(b). The equations of motion for the body of interest are

$$\ddot{\bar{\rho}}_{ci} = -G\left(\frac{m_i + m_c}{||\bar{\rho}_{ci}||^3}\right)\bar{\rho}_{ci} + G\sum_{\substack{k=1 \\ k\neq i,c}}^{\mathrm{N}} m_k\left(\frac{\bar{\rho}_{ck} - \bar{\rho}_{ci}}{||\bar{\rho}_{ck} - \bar{\rho}_{ci}||^3} - \frac{\bar{\rho}_{ck}}{||\bar{\rho}_{ck}||^3}\right) \tag{8}$$

where G is the gravitational constant and m_γ is the mass of the P_γ body. Note that the state vector for the P_k perturbing body with respect to the central body P_c, that is, $\bar{\rho}_{ck}$, is accessed using the Jet Propulsion Laboratory DE430 ephemerides via the SPICE toolkit [8]. The ephemeris formulation in the current investigation includes the Earth, the Moon, the Sun, and Jupiter. The equilibrium points derived in the lower-fidelity models, such as the L_i libration points in the CR3BP, do not exist in the ephemeris model. However, quasi-periodic motion in the vicinity of these points may still exist in the higher-fidelity ephemeris model.

B. Near Rectilinear Halo Orbits

The halo family and its subset, the NRHOs, are comprised of three-dimensional precisely periodic orbits as defined in the CR3BP. The halo family bifurcates from each family of planar Lyapunov orbits associated with the collinear libration points. For the L_1 and the L_2 equilibrium points in the Earth-Moon system, the halo family originates in the x-y plane from the bifurcation orbit in the Lyapunov family and evolves out-of-plane as the family of orbits approaches the Moon. Note that the halo family is mirrored across the x-y plane; members of the northern family possess a positive z value over the majority of their orbit, while the southern family members are defined by a negative z component. Representative southern L_1 and L_2 halo orbits in the Earth-Moon CR3BP appear in Fig. 2 colored as a function of the orbital period. The orbits in bold red denote the boundaries of the NRHO subset for each family. Zimovan et al. [9, 10] define the bounds on the NRHO subsets for the L_1 and L_2 families by their linear stability properties. The Earth-Moon L_1 and L_2 halo families are precisely periodic orbits in the CR3BP.

The Earth-Moon-Sun BCR4BP is formulated to represent a time-dependent, periodic system. Therefore, only isolated periodic orbits with specific periods exist rather than families with continuously varying periods [11]. While periodic solutions in the CR3BP only require periodicity in 6 states, i.e, the position and velocity states, solutions in the BCR4BP require an additional condition, that is, the Sun location must also be commensurate with the periodic cycle [5, 12]. Thus, the period for any precisely periodic orbit in the BCR4BP is an integer multiple of the Earth-Moon-Sun synodic period, that is, approximately 29.5 days. Periodic orbits with an orbital period equal to a rational fraction of the synodic period are denoted synodic resonant periodic orbits in the CR3BP and the BCR4BP. Boudad et al. [12, 13] investigate the transition of synodic resonant L_2 NRHOs from the Earth-Moon CR3BP to the Earth-Moon-Sun BCR4BP. A sample of four synodic resonant NRHOs are plotted in Fig. 3. The four periodic orbits in Fig. 3(a) are constructed in the Earth-Moon CR3BP and are the basis for the construction of a periodic solution in the BCR4BP via a continuation/corrections procedure [5, 12]. The results of the transition process are precisely periodic orbits in the BCR4BP and appear in Fig. 3(b). The X:1 synodic orbits are continued to T_{syn}-periodic orbits in the BCR4BP, and the 9:2 NRHO is continued to a $2T_{\text{syn}}$-periodic orbit. The geometry and the apse distance to the Moon are generally maintained during the continuation process, as apparent in Fig. 3. Synodic resonant periodic orbits, including halo orbits and NRHOs, in the Earth-Moon CR3BP are transitioned to precisely periodic orbits in the Earth-Moon-Sun BCR4BP.

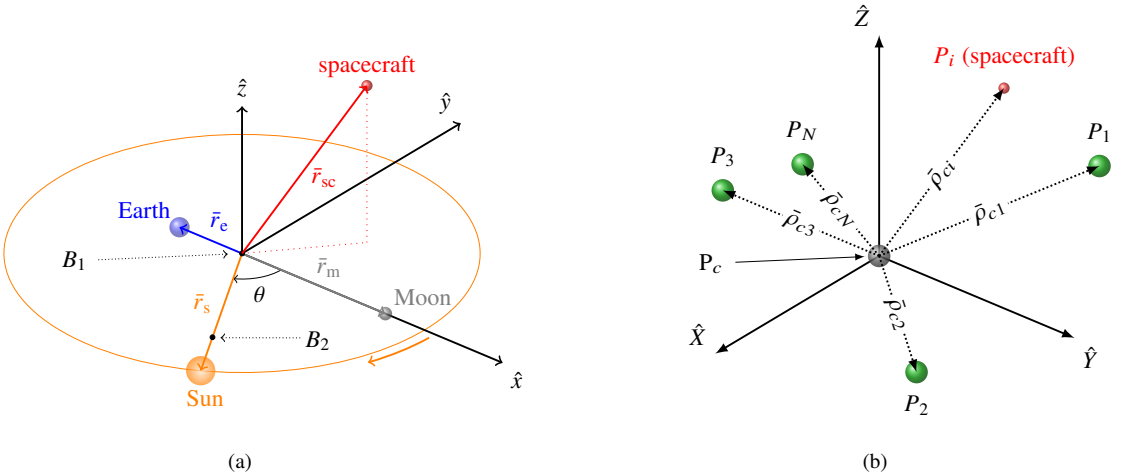

Fig. 1 BCR4BP as formulated in the Earth-Moon rotating frame (a). N-Body ephemeris model as defined in the P_c-centered inertial frame.

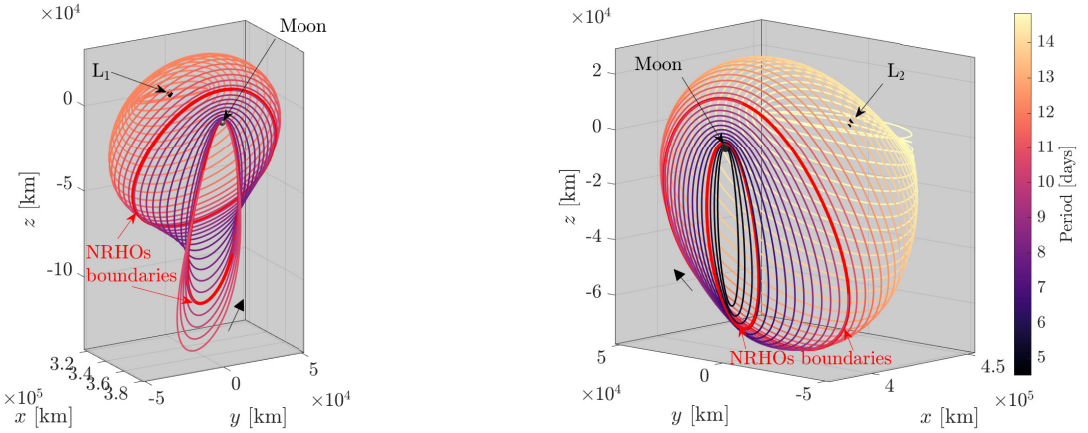

Fig. 2 Representative 3D members of the CR3BP Earth-Moon L_1 (a) and L_2 (b) halo families, colored as a function of the orbital period. Orbits in bold red denote the boundaries of the NRHO subset in each family.

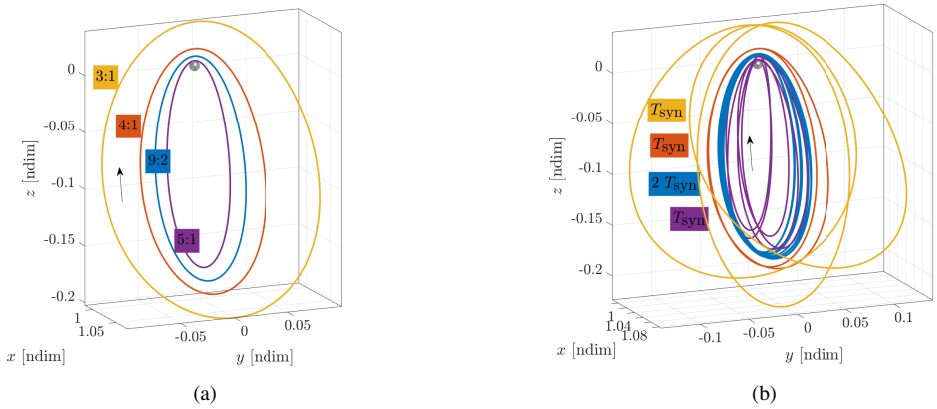

Fig. 3 Four synodic resonant L_2 NRHOs as viewed in the Earth-Moon rotating frame, computed in the Earth-Moon CR3BP (a) and in the Earth-Moon-Sun BCR4BP (b).

III. Motivation

The process for transitioning a solution from the CR3BP to the ephemeris is not unique, that is, there are multiple processes that generate converged solutions with different characteristics in the ephemeris model. Recall that the ephemeris model relies on ephemerides for the position, velocity, and epoch states of the celestial bodies. Consequently, the ephemeris model is not time-autonomous, like the CR3BP; nor is it time-dependent and periodic like the BCR4BP. Periodic orbits from lower-fidelity models, that is, the CR3BP or the BCR4BP, are thus transitioned to a bounded or, at best, quasi-periodic motion in the ephemeris model. As such, without careful consideration of the details of the transitioning process, an infinite variety of trajectories may emerge. One transition approach to shift a periodic orbit between models involves a stacking process [14]. Multiple revolutions of the periodic orbit from the CR3BP (or the BCR4BP) are stacked, discretized, and corrected for continuity in the ephemeris model using a differential corrections scheme. However, periodicity is not enforced: the initial and final states along the corrected ephemeris trajectory do not necessarily match. When multiple revolutions from the same orbit are stacked together, the strategy is labeled a 'homogeneous stacking' scheme. Previous contributions offer details for the development of 'non-homogeneous stacking' strategies, where different orbits from the CR3BP are stacked together to create the initial guess for the higher-fidelity model for the purpose of achieving certain specific characteristics in the converged final orbit, such as the

perilune epoch [15] or the perilune radius [7]. The present investigation leverages a homogeneous stacking method to transition periodic orbits in the CR3BP to bounded motions in the ephemeris model.

The transition of a periodic orbit from the CR3BP to the ephemeris model is not always successful, i.e., key characteristics from the CR3BP motion are not always maintained in the higher-fidelity model. For instance, consider the trajectories in Fig. 4. Four L_2 halo orbits are transitioned from the Earth-Moon CR3BP to the Earth-Moon-Sun-Jupiter ephemeris model. Recall that in this formulation of the ephemeris model, the celestial bodies are included as point masses. The four selected halo orbits are characterized by synodic resonant periods; each period is a rational multiple of the synodic period, that is, approximately 29.5 days. In this example, the 2:1, 3:1, 9:2, and 5:1 synodic resonant L_2 halo orbits are selected. Their associated orbital periods are equal to $1/2$, $1/3$, $2/9$, and $1/5$ of the synodic period, respectively. For each orbit, 12 revolutions are stacked and the epoch for the initial state is set to May 15th, 2023. The resulting trajectories are discretized; patch points are selected every 2 days and propagated without corrections in the ephemeris model. The resulting initial guesses that are not converged in the ephemeris are plotted as viewed in the Earth-Moon rotating frame in Fig. 4(a). The trajectories are discontinuous, as highlighted by the insert in Fig. 4(a). Thus, a differential corrections scheme is employed to enforce continuity in position, velocity, and epoch between consecutive arcs. The resulting converged bounded motions are plotted in Fig. 4(b). For the 2:1 halo orbit, the 9:2 NRHO, and the 5:1 halo orbit, the ballistic trajectories as constructed in the ephemeris model remain in close vicinity in configuration space of the CR3BP periodic orbits, plotted as the black dashed lines in Fig. 4(b). (Note the CR3BP periodic orbits are also plotted for reference in Fig. 4(a), but are indistinguishable given the initial guesses propagated in the ephemeris model.) However, the geometry of the 3:1 NRHO is not maintained in the ephemeris model. The trajectory that results from the differential corrections scheme, plotted in red in Fig. 4(b), does not resemble the 3:1 NRHO from the Earth-Moon CR3BP, denoted by the black dashed line, or even the initial guess in the ephemeris model, plotted in red in Fig. 4(a). The ephemeris trajectory from the differential corrections scheme is continuous in position, velocity, and epoch, and remains in the vicinity of the Moon, but does not follow any bounded pattern. In this example, at this epoch, the 3:1 L_2 NRHO is not successfully transitioned from the Earth-Moon CR3BP to the Earth-Moon-Sun-Jupiter ephemeris model.

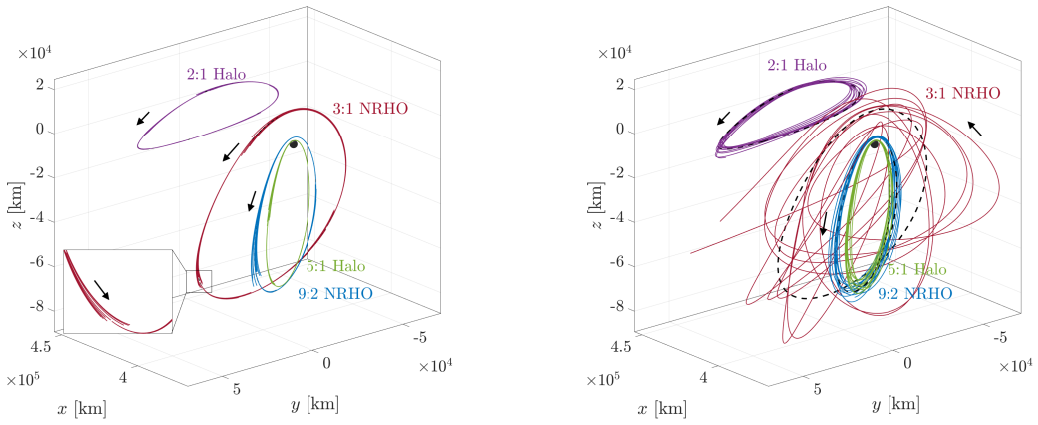

(a) Initial guesses

(b) Converged trajectories

Fig. 4 Initial arcs (a) and converged trajectories (b) for various Earth-Moon L_2 halo orbits, as computed in the Earth-Moon-Sun-Jupiter ephemeris model and plotted in the Earth-Moon rotating frame. The initial guesses are constructed leveraging CR3BP periodic orbits.

To examine the 3:1 NRHO transition discrepancies, the characteristics of the four Earth-Moon halo orbits from Fig. 4 are explored in the CR3BP. The orbital periods, perilune radii, and stability information associated with these four orbits as computed in the CR3BP are summarized in Table 1. One may assume that the proximity of the CR3BP orbit to the Moon determines the quality of the transition to the ephemeris model. Such is not the case in this example, where the 2:1 halo, 9:2 NRHO, and 5:1 halo orbit are defined with perilune radius ranging from approximately 1,600 km to 50,000 km, and are favorably transitioned to the ephemeris model. (Note the perilune radius associated with the 5:1 halo

Table 1 Characteristics of the Earth-Moon CR3BP halo orbits prior to transition to the ephemeris model in Fig. 4.

Orbit	5:1 Halo	9:2 NRHO	3:1 NRHO	2:1 Halo Orbit
Period [days]	5.90	6.55	9.83	14.74
Perilune radius [km]	1,694	3,223	15,138	49,321
Magnitude of	0	0.5157	0	2.0366
the Lyapunov	0	0	0	0
exponents	0	0	0	0
Linear stability	stable	unstable	stable	unstable

orbit is within the radius of the Moon, but all bodies are assumed to be point masses in the dynamical models employed in this investigation.) However, while the perilune radius along the 3:1 NRHO lies between the radii associated with the 2:1 halo and 9:2 NRHO, the geometry of this NRHO is not maintained when shifted to the higher-fidelity model in this example. The stability (in the linear sense) associated with the CR3BP periodic solution is also explored. In this investigation, stability is defined in terms of the Lyapunov exponent associated with the monodromy matrix, i.e., the state-transition matrix evaluated after one orbital period along the periodic solution. The Lyapunov exponent is labeled ϕ_i, and is defined as the real part of the Floquet exponent, that is,

$$\phi_i = \Re\left(\frac{\ln \lambda_i}{T}\right) \tag{9}$$

where T is the period of the orbit and the λ_i is the i-th eigenvalue of the monodromy matrix associated the periodic solution. The phase space in the CR3BP is six-dimensional, thus, the monodromy matrix corresponding to a periodic solution admits six eigenvalues and, thus, six Lyapunov exponents. A periodic solution in the CR3BP possesses a pair of eigenvalues equal to one due to the Jacobi constant and the time-autonomous nature of the CR3BP [3, 16]. Thus, two of the Lyapunov exponents are equal to zero. The zero Lyapunov exponents correspond to the absence of expansion (quantified by positive Lyapunov exponents), or contraction (quantified by negative Lyapunov exponents) when a perturbation is introduced along the direction of the trajectory. Recall, from the Lyapunov theorem [17], that eigenvalues occur in reciprocal pairs if they are real or in conjugate pairs if they are complex. As a consequence, a positive Lyapunov exponent is always accompanied by a negative Lyapunov exponent. Therefore, the necessary condition for linear stability of a periodic orbit in the CR3BP is that all the Lyapunov exponents must be equal to zero. From Table 1, the 2:1 halo and the 9:2 NRHO are unstable in the linear sense, as evidenced by the Lyapunov exponents with non-zero magnitudes. However, in contrast to the 2:1 halo, the 9:2 NRHO does not possess well-defined manifold structures [18] and is sometimes labeled a 'nearly-stable' orbit. In contrast, all of the Lyapunov exponents associated with the 3:1 halo orbit and the 5:1 halo orbit are equal to zero; the orbits are, thus, considered stable in the linear sense. Note that there is no apparent relationship between the linear stability and the ephemeris solution that is constructed with the current scheme: while the 5:1 halo orbit and the 3:1 NRHO are linearly stable, only the geometry of the 5:1 halo is generally maintained when the orbit is transitioned to the higher-fidelity, ephemeris model. The challenges in maintaining the geometry of the Earth-Moon 3:1 NRHO when transitioning it the ephemeris model are not apparently related to its orbital and stability characteristics.

The proximity of the 3:1 NRHO to bifurcations that result in the existence other families of periodic orbits is investigated. Within the context of the CR3BP, a bifurcation point is an orbit along a family of periodic orbits that may 'branch' into a new family of periodic solutions [19]. For instance, the halo families of periodic orbits emerge from bifurcating orbits along the Lyapunov families associated with each collinear equilibrium points in the CR3BP. At a bifurcation, the linear stability properties associated with the periodic mode may change. However, bifurcations without any change in stability are also possible. The proximity of the 3:1 NRHO to bifurcations along the L_2 halo family that introduce stability changes is explored in Fig. 5(a). The Lyapunov exponents along a subset of the L_2 halo family is plotted as a function of the perilune radius. As the selected stability index, the Lyapunov exponent is an apt metric to detect bifurcations associated with a change in stability. Tangent and period-doubling bifurcations [20], denoted by cyan and magenta clubs symbols, respectively, in Fig. 5(a), are two types of bifurcations with stability changes. At each of the highlighted locations, one curve (or multiple curves) intercepts the $\phi = 0$ line. (Note that the changes in Lyapunov exponents associated the rightmost period-doubling bifurcation are indistinguishable at this scale.) Recall that

the NRHO subset is defined as the set of halo orbits that are located between the first and third stability changes along the family of periodic solutions, in the direction of increasing perilune radius; the NRHO subset is plotted in bold black in Fig. 5(a). Since all of its associated Lyapunov exponents are equal to zero, the 3:1 NRHO is a stable (in the linear sense) member of the L_2 halo family of orbits. However, the 3:1 NRHO is surrounded by a period-doubling bifurcation in the direction of decreasing perilune radius and by a tangent bifurcation in the direction of increasing perilune radius, as apparent in Fig. 5(a). Bifurcations that do not involve a change in the linear stability properties of the family of orbits are explored in Fig. 5(b). Period-multiplying bifurcations occur when the non-trivial eigenvalues of the monodromy matrix encounter a n-th root of unity [21]. Thus, these bifurcations are identified by examining the angles formed by the real axis of the complex plane and the eigenvalues, i.e., $\Im\left(\log(\lambda_i)\right)$. Period-multiplying bifurcations occur when one of the angles crosses a rational fraction of 2π. For instance, the horizontal dashed line at $2\pi/3$ rad = 120 deg in Fig. 5(b) is employed to identify period-tripling bifurcations. The complex dynamical neighborhood of the 3:1 NRHO may explain some of the challenges associated with the transition to the ephemeris model. Note that the period-doubling type of

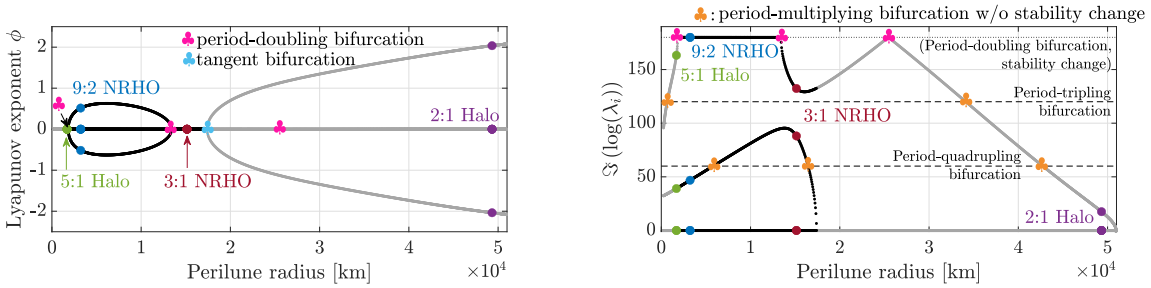

(a) Bifurcations with stability change

(b) Bifurcations without stability change

Fig. 5 Locations of selected bifurcations with stability change (a) and bifurcations without stability change (b) along a subset of the CR3BP L_2 halo family of periodic orbits.

bifurcations, denoted by the magenta clubs symbols in both plots in Fig. 5 is a specific type of period-multiplying bifurcation that involves a change of the linear stability properties along the family. Period-multiplying bifurcations without stability changes are represented by the orange clubs symbols in Fig. 5(b). The 3:1 NRHO is in proximity of a period-quadrupling bifurcation along the family in the direction of increasing perilune radius. Campbell [19] and Zimovan-Spreen [22] have explored the families of periodic orbits that emerge from the bifurcations along the Earth-Moon L_2 halo family, including the bifurcations located near the 3:1 NRHO. The bifurcating orbits identified in Fig. 5 are plotted in configuration space in Fig. 6: the 3:1 NRHO, plotted in red, is surrounded by the period-doubling bifurcating orbit on one side and by the period-quadrupling and tangent bifurcating orbits on the other side.

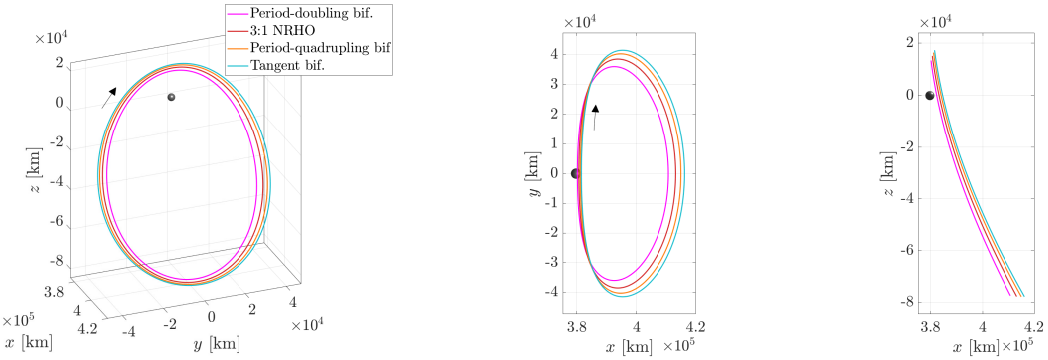

(a)

(b) Top-down view

(c) Side view

Fig. 6 Bifurcating orbits in the vicinity of the CR3BP L_2 synodic resonant 3:1 NRHO, as viewed in the Earth-Moon rotating frame.

For specific epochs, the 3:1 NRHO from the Earth-Moon CR3BP is transitioned to a bounded motion in the ephemeris model. However, the geometry of the ephemeris transition orbit that is constructed does not resemble the one from the lower-fidelity model, that is, the CR3BP. For instance, consider the trajectories plotted in Figs. 7(a)–7(c). For this example, 9 revolutions of the 3:1 NRHO as computed in the Earth-Moon CR3BP are discretized and corrected for continuity in the Earth-Moon-Sun-Jupiter ephemeris model. The epoch associated with the initial guess is varied; the epochs of the three trajectories in Figs. 7(a)–7(c) are selected 5 days apart during the month of May 2023. In Figs. 7(a) and 7(c), no clear pattern in the constructed ephemeris motion appears. However, for the trajectory originating on May 17, 2023, the nine revolutions of the orbits are consistently distributed in a three-lobe geometry. This three-lobe geometry was first identified by Davis et al. [23], who labeled it the 'tightly converged geometry' while the geometries from Figs. 7(a) and 7(c) are 'loosely converged'. A bounded motion geometry that does not resemble the CR3BP 3:1 NRHO is produced in the ephemeris model for certain epochs. Even though the synodic resonant 3:1 NRHO is a linearly stable orbit, it exists in a dynamically complex environment and is located in the close vicinity of multiple bifurcations.

The tightly converged geometry for the 3:1 NRHO constructed in the ephemeris model resembles the 3:1 NRHO as computed in the BCR4BP. The trajectories plotted in Figs. 7(a)–7(c) are constructed using the CR3BP 3:1 NRHO, plotted in blue in Fig. 7(d). However, the tightly converged trajectory for the epoch of May 17, 2023 in Fig. 7(c) distinctly resembles the 3:1 NRHO as computed in the Earth-Moon-Sun BCR4BP, plotted in orange in Fig. 7(d). Therefore, leveraging the BCR4BP periodic orbit is proposed as an intermediate step to construct an ephemeris trajectory corresponding to the Earth-Moon 3:1 CR3BP. Additionally, information from the periodic solutions from the BCR4BP is leveraged to guide the transition process.

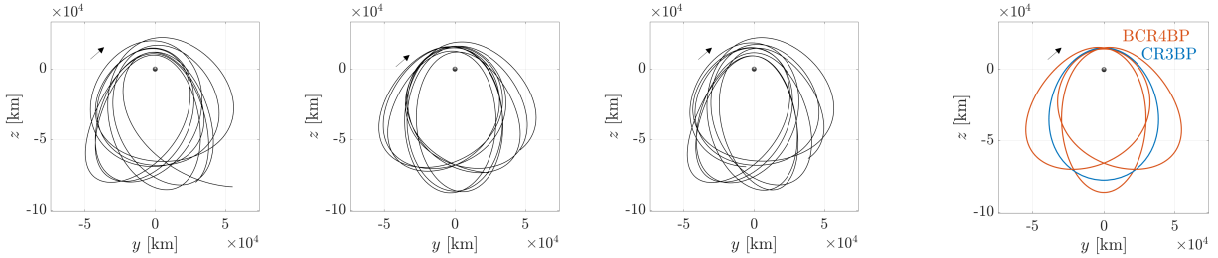

(a) May 12, 2023 (b) May 17, 2023 (c) May 22, 2023 (d) Lower-fidelity solutions

Fig. 7 Converged solutions for 9 revolutions of the 3:1 synodic resonant in the Earth-Moon-Sun-Jupiter ephemeris model, leveraging the CR3BP periodic orbit for the initial guesses (a,b,c). 3:1 synodic resonant NRHO in the Earth-Moon CR3BP and the Earth-Moon-Sun BCR4BP (d). All orbits are viewed in the Earth-Moon rotating frame, down the $\hat{x}$ axis.

IV. Methodology

A. 3:1 Synodic Resonant NRHO in the BCR4BP

The BCR4BP 3:1 NRHO is employed as an intermediate step in the continuation process between the CR3BP and the ephemeris model. Previous authors [5, 12] have investigated the process for transitioning a synodic resonant periodic orbit from the CR3BP to the BCR4BP. The BCR4BP periodic orbit corresponding to the 3:1 NRHO in the CR3BP is plotted in various frames in Fig. 8. When the BCR4BP orbit is viewed in the Earth-Moon rotating frame, as in Fig. 8(a), the three distinct lobes observed in the ephemeris solution in Fig. 7(c) are apparent. The 'left' lobe is labelled 'L' and is stretched in the $+\hat{y}$ direction. Conversely, the 'right' lobe, stretched in the $\hat{y}$ direction, is denoted 'R'. Finally, the remaining lobe is centered along the rotating $\hat{x}$ axis and labeled 'C' in Fig. 8(a). The 3:1 NRHO as computed in the CR3BP is similarly centered along the rotating $\hat{x}$ axis; it appears in purple in Fig. 8(a). Apolunes associated with the CR3BP and the BCR4BP periodic solutions are represented by an inverted triangle in Fig. 8. Note the color scheme associated with the L, C, and R lobes; this scheme is employed throughout the rest of this investigation to identify each lobe. The effects of the solar gravitational influence on the 3:1 NRHO are particularly visible when the orbit is plotted in an arbitrary Moon-centered inertial frame and viewed from the top, as in Fig. 8(b). The 3:1 NRHO as computed in the CR3BP is propagated for three revolutions and plotted in purple. Similar to the BCR4BP periodic solution, plotted in black in Fig. 8(b), the CR3BP 3:1 NRHO possesses three distinct lobes when represented in this frame. When the

gravitational influence of the Sun is included in the dynamical model, the original three lobes from the CR3BP are pulled in different directions, resulting in the distinct three-lobe geometry associated with the BCR4BP periodic orbit plotted in Fig. 8(a).

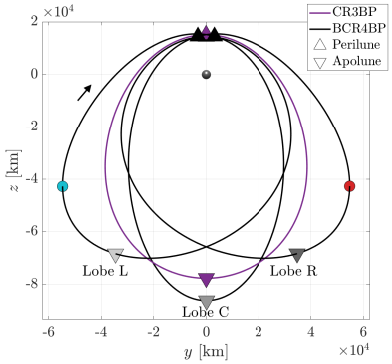

(a) Earth-Moon rotating frame, looking toward the Earth

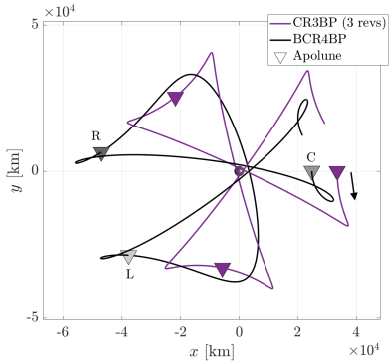

(b) Arbitrary Moon-centered inertial frame, top-down view

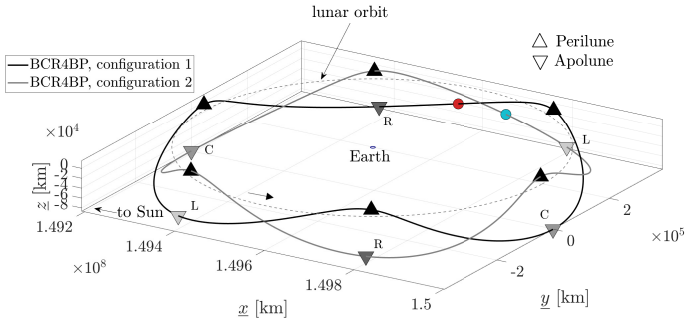

(c) Sun-B_1 rotating frame

Fig. 8 Geometry of the 3:1 NRHO computed in the BCR4BP, as viewed in the Earth-Moon rotating frame (a), in an arbitrary Moon-centered inertial frame (b), and in the Sun-B_1 rotating frame (c). Perilunes are denoted by a triangle, apolunes are denoted by an upside-down triangle. For the BCR4BP orbit, the apolunes are colored according to their lobe: 'L' in light gray, 'C' in gray, 'R' in dark gray. Two spacecraft, identified by the cyan and red circles in Figs. 8(a) and 8(c) are concurrently flying in the BCR4BP 3:1 NRHO, one in each configuration.

The 3:1 NRHO computed in the BCR4BP exists at two different epochs, or 'configurations'. Recall that the BCR4BP is a time-dependent, periodic model. The epoch is defined as the Sun angle θ, that is, the angle between the Earth-Moon rotating $\hat{x}$ axis and the Sun position vector, as defined in Fig. 1(a). A periodic solution in the BCR4BP exists for one or multiple initial Earth-Moon-Sun relative orientations, or configurations [12]. The solutions at different configurations are apparent when plotted in the Sun-B_1 rotating frame [7]. The Sun-B_1 rotating frame is the BCR4BP analog of the CR3BP Sun-Earth rotating frame. In this frame, the Sun and the Earth-Moon barycenter, that is, B_1, are fixed while the Earth and the Moon are in circular orbits around B_1. The 3:1 NRHO as computed in the BCR4BP exists in two different configurations; the two resulting orbits are plotted as viewed in the Sun-B_1 rotating frame in Fig. 8(c). The lunar orbit is represented by the dashed black line, and perilune and apolunes are denoted by triangles and inverted triangles, respectively. Due to the symmetric nature of the BCR4BP, the apolune associated with the center lobe (C), colored in gray, is located along the Sun-B_1 rotating $\hat{\underline{x}}$ direction for each configuration. However, in the Sun-B_1 rotating frame, the apolune C is located on the right of the Earth for configuration 1, and on the left of the Earth for configuration 2. The apolunes associated with the remaining two lobes are colored in dark gray for the right (R) lobe and light gray for the left (L) lobe in Fig. 8(c). From the view in the Sun-B_1 rotating frame, it is apparent that the solutions from the two different configurations are rotated from each other by 180° around the rotating $\hat{\underline{z}}$ axis. The Sun angles associated with the apolunes of each solution are summarized in Table 2. Consistent with the observation in Fig. 8(c), that is, the Sun

angles at apolune are shifted by precisely 180° between the two configurations. The periodic solutions corresponding to the two configurations overlap when the orbits are plotted in the Earth-Moon rotating frames; both solutions coincide with the orbit plotted in black in Fig. 8(a). Note that two spacecraft can fly concurrently in the BCR4BP 3:1 NRHO: one spacecraft along the orbit associated with configuration 1, and the other along the orbit given configuration 2. As an illustration, consider the red and cyan circles in Figs. 8(a) and 8(c). The red circle represents a spacecraft flying in the 3:1 NRHO in configuration 1 while the blue circle represents a spacecraft flying in the 3:1 NRHO in configuration 2 *at the same instant in time*. While the spacecraft denoted by the red circle is approaching apolune along the R lobe, the blue dot spacecraft is approaching perilune along the L lobe, as apparent in Fig. 8(a). Note that the two 3:1 NRHOs at different configurations do not intersect when viewed in the Sun-B_1 rotating frame, as Fig. 8(c) might suggest. The 'intersection' point corresponds to the closest approach between the gray and black curves in Fig. 8(c): the two spacecraft are then located at the same z coordinate, but on different sides of the Earth-Moon rotating $\hat{x}$ axis in Fig. 8(a). The 3:1 NRHO as computed in the BCR4BP exists at two different epochs; two spacecraft can contemporaneously fly along the 3:1 NRHO without encountering each other.

B. Epoch transformation between the BCR4BP and Ephemeris Model

The process employed in this investigation to convert between a BCR4BP epoch, that is, a specific value of Sun angle, and the epoch employed in the ephemeris force model is detailed. Recall that the BCR4BP is a time-dependent model, as is the ephemeris model. However, the BCR4BP is a periodic model, of period equal to the lunar synodic month. Thus, a Sun-Earth-Moon configuration represented by a certain Sun angle corresponds to an infinite number of epochs in the higher-fidelity ephemeris model. For instance, a Sun angle equal to 180° corresponds to an alignment of the Sun, the Earth, and the Moon, in this order. This configuration also corresponds to the first phase of the lunar cycle, that is, a new Moon. Thus, the Sun angle $\theta = 180°$ corresponds to all possible new Moon epochs. Since the BCR4BP is a periodic dynamical model, the conversion of the epoch from the BCR4BP to the ephemeris force model is not unique.

For practical reasons, the Sun angle in the BCR4BP is matched to an epoch given a specific month and a specific year. For instance, the Sun angle $\theta = 180°$ is mapped to a unique epoch for the month of February 2020. The month and year are selected to be as close as possible to the desired epoch in the ephemeris model. To determine the day within the month and year that corresponds to the BCR4BP configuration, the osculating Sun angle is computed over this range as

$$\hat{\theta} = \arccos\left(\frac{\bar{\rho}^R_{\text{B1-Moon}} \cdot \bar{\rho}^R_{\text{B1-Sun}}}{\|\bar{\rho}^R_{\text{B1-Moon}}\|\|\bar{\rho}^R_{\text{B1-Sun}}\|}\right) \tag{10}$$

where $\bar{\rho}^R_{\text{B1-}i}$ is the position vector from the Earth-Moon barycenter to the body i, obtained from ephemerides and rotated to the Earth-Moon rotating frame. Then the corresponding epoch is determined in the ephemeris by locating the epoch corresponding the minimum error between the Sun angle in the BCR4BP and the osculating Sun angle as computed in the ephemeris model, that is,

$$\text{equivalent epoch} = \arg\min_{\substack{\text{month,}\\ \text{year}}} \left(|\theta - \hat{\theta}|\right) \tag{11}$$

Some assumptions are incorporated when employing this conversion process between epochs in the ephemeris and the BCR4BP. First, the Sun position vector employed in Eq. (10) to compute the osculating Sun angle is generally not in the Earth-Moon plane, since the Earth, Moon, and Sun are not located in the same plane in the ephemeris model. Thus, the equivalent epoch in Eq. (11) is computed by comparing angles defined in two different planes. However, note that this approximation is acceptable for the Earth-Moon-Sun system, as the mean inclination of the lunar orbit with respect to the ecliptic plane is approximately 5.14°. For instance, the conversion method, described in Eqs. (10) and (11) and tested for the month of February 2020, predicts a new Moon ($\theta = 180°$) on the 09th at 07:47 UTC. According the NASA GSFC Sky Events Calendar [24], a new Moon occurred on February 09th at 07:33 UTC. Thus, the simplified scheme is a suitable approximation for converting between ephemeris and BCR4BP epochs. The second assumption maps each Sun angle to one epoch for a given month and year. In reality, this mapping is not always unique, since the lunar synodic month (approximately 29.5 days) is shorter than the mean month-length (30.4 days). Thus, for certain months, a specific Sun angle corresponds to two different days. For instance, a new Moon ($\theta = 180°$) occurs on both the 1st and the 30th day in April 2022. In such instances, the strategy in Eqs. (10) and (11) returns the epoch that is numerically the closest to the selected Sun angle θ. The equivalent epochs for the apolunes in the BCR4BP 3:1 NRHO as plotted in Fig. 8 are computed for the month of May 2023 using the technique described in Eqs. (10) and (11) and are included in Table 2. The method procedure in this investigation maps an epoch as defined in the BCR4BP, that is, a Sun angle value, to an epoch in the ephemeris model given a certain month and year.

Table 2 Sun angle and equivalent epochs for the month of May 2023 for the two configurations of BCR4BP 3:1 NRHOs plotted in Fig. 8(c).

Configuration	**1**		**2**	
Lobe	Sun angle, deg	Equivalent Epoch	Sun angle, deg	Equivalent Epoch
L	−64	2023 MAY 25 05:44:30	116	2023 MAY 10 15:18:11
C	180	2023 MAY 05 17:33:41	0	2023 MAY 19 15:16:45
R	64	2023 MAY 14 14:03:14	−116	2023 MAY 29 23:18:11

C. Apse Angle

To assess the quality of a trajectory transitioned to the ephemeris model from the CR3BP, a metric, the apse angle [25], is employed in this investigation. Recall that periodic solutions from the CR3BP or the BCR4BP evolve into a quasi-periodic orbit, or bounded motion, in the ephemeris model. The solutions constructed in the ephemeris model may be 'tightly converged', as the bounded solution in Fig. 7(b), or 'loosely converged', as the trajectories in Figs. 7(a) and 7(c). While many metrics are available to assess the quality of a converged solution, the apse angle is particularly suitable for the NRHOs. The apse angle is defined in this investigation, in the Earth-Moon rotating frame, as the angle between the projection of an apolune in the $\hat{y}$-$\hat{z}$ plane and the rotating $-\hat{z}$ axis, i.e.,

$$\alpha = \arctan\left(-\frac{y_{\text{apolune}}}{z_{\text{apolune}}}\right) \tag{12}$$

The apse angles associated with the 3:1 NRHO in the CR3BP and the BCR4BP propagated for three synodic months are noted in Figs. 9(a) and 9(b). Since the apolune of the 3:1 NRHO as computed in the CR3BP, denoted by the purple inverted triangles in Fig. 9(a), is located on the Earth-Moon rotating $\hat{z}$ axis, the apse angle associated with the orbit remains equal to zero for the nine revolutions included in Fig. 9(b). Conversely, the analog to the 3:1 NRHO in the BCR4BP, plotted in black in Figs. 9(a) and 9(b), possesses the distinct three-lobe geometry. Thus, the apse angles over the two synodic months present a clear pattern, that is, a succession of a negative apse angle values around −25° for the L lobe, a 0° apse angle for the central lobe, C, and a positive apse angle value around +25° for the lobe R. The pattern of the apse angle evolution along the 3:1 NRHO remains constant when the orbit is computed in the lower-fidelity model, i.e., the CR3BP and the BCR4BP.

The apse angle is employed to determine the 'boundedness' of an analog to the 3:1 CR3BP as constructed in the ephemeris model. Consider the two bounded motions computed in the Earth-Moon-Sun-Jupiter ephemeris model in Fig. 9(c). The trajectory plotted in black corresponds to the 'tightly converged' geometry; three distinct groups of lobes and, thus, three distinct groups of apolunes (denoted by black inverted triangles in Fig. 9(c)) are apparent. The apse angles associated with this trajectory are plotted in black in Fig. 9(d). Note that the pattern of the apse angles closely resembles the one associated with the BCR4BP in Fig. 9(b). For reference, the apse angles associated with the BCR4BP orbits, $\alpha_{L,4}$, $\alpha_{C,4}$, and $\alpha_{R,4}$ are included as the gray horizontal lines in Figs. 9(b) and 9(d). As a comparison, a 'loosely converged' NRHO computed in the ephemeris model is plotted in blue in Fig. 9(c). The lobes associated with this solution appear to be arbitrarily distributed, and there is not an apparent pattern grouping the apolunes, plotted as the blue inverted triangles in Fig. 9(c). Consequently, the apse angles plotted as a function of the epoch in Fig. 9(d) appear randomly distributed. Plotting the apse angles as a function of time along the trajectory, or equivalently, as a function of epoch, provides visual insight on the quality of a solution transitioned from a lower-fidelity model to the ephemeris model.

To quantify the boundedness of a 3:1 NRHO analog in the ephemeris model, the mean and standard deviation for the apse angles associated with each lobe of a trajectory are examined. The mean value provides information on the location of each lobe, while the standard deviation describes the spread of each lobe. As an illustration, the mean and standard deviation of the apse angles along the trajectories in Fig. 9 are summarized in Table 3. First, the standard deviations associated with all the apse angle values in the BCR4BP are all equal to zero. Since the orbit is exactly periodic in this model, consecutive revolutions overlap each other. (Note that the both the mean and standard deviation associated with the CR3BP NRHO are equal to zero). For the analogs to the 3:1 NRHO that are 'tightly' converged in the ephemeris model, the geometry of the lobes mostly repeats each synodic month. Thus, the standard deviation of the apse angles is small: 2.21° for the L lobe, 1.16° for the C lobe, and 0.72° for the R lobe. Further, each group of lobes is relatively close to its BCR4BP counterpart, as evidenced by the mean values of the apse angles in Table 3. Conversely,

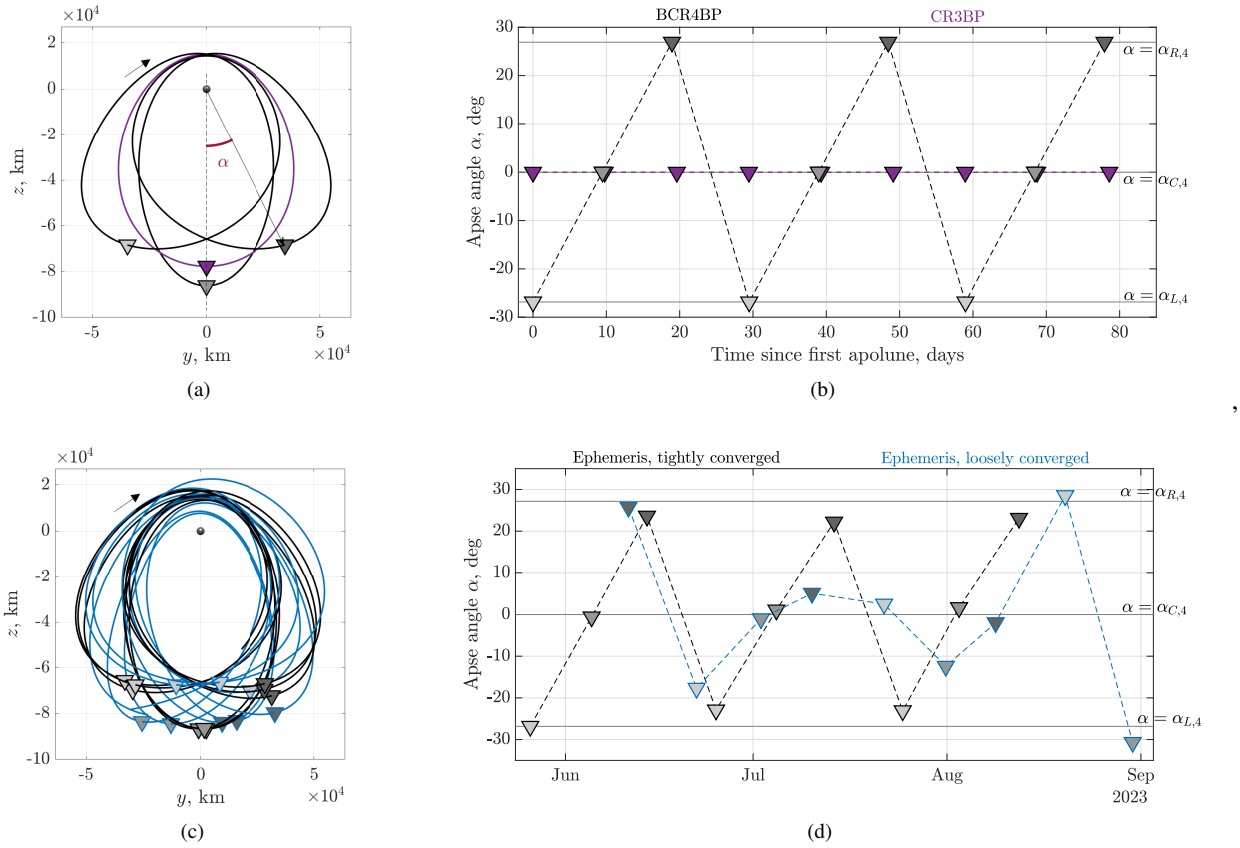

Fig. 9 Apse angle associated with the 3:1 NRHO in the lower-fidelity models (a,b) and for two initial epochs in the ephemeris model (c,d) for a three-month propagation. A 'tightly converged' trajectory, plotted in black, and a 'loosely converged' trajectory, plotted in blue, are obtained in the ephemeris model.

the mean values associated with the 'loosely' converged orbit in Figs. 9(a) and 9(b) are very different from the values associated with the 3:1 NRHO as computed in the BCR4BP. Additionally, the standard deviation associated with each group is substantial (over 14°), which indicates a high variation between apse angle values. In the ephemeris model, a 'tightly' converged analog to the 3:1 NRHO is defined by the following conditions:

1) The apolunes are evenly distributed in three groups: $|\bar{\alpha}_L| \approx |\bar{\alpha}_R|$ and $\bar{\alpha}_C \approx 0$
2) In each group, the lobes are not spread out: $\sigma_{\alpha,L}, \sigma_{\alpha,C}, \sigma_{\alpha,R} \leq \sigma_{max}$

The maximum standard deviation, σ_{max}, is set to 3° in this investigation. Note that this value depends on the application of interest: certain scenarios may require a 'tighter' distribution of the apolunes (a lower value for σ_{max}) while a larger spread of the apolunes (higher σ_{max} value) might be allowable in other scenarios. Rather than relying on visual inspection, the mean and standard deviations associated with the apse angles supply a metric to define the boundedness of a 3:1 analog in the ephemeris model.

Table 3 Mean ($\bar{\alpha}_i$) and standard deviation ($\sigma_{\alpha,i}$) of the apse angles associated with the trajectories plotted in Fig. 9.

	Lobe L		Lobe C		Lobe R	
Dynamical model	$\bar{\alpha}_L$ (deg)	$\sigma_{\alpha,L}$ (deg)	$\bar{\alpha}_C$ (deg)	$\sigma_{\alpha,C}$ (deg)	$\bar{\alpha}_R$ (deg)	$\sigma_{\alpha,R}$ (deg)
BCR4BP	−26.85	0	0	0	26.85	0
Ephem., tightly converged	−24.27	2.21	0.72	1.16	22.95	0.72
Ephem., loosely converged	4.44	23.17	−14.71	14.97	9.63	14.40

V. Results

The periodic orbits constructed in the BCR4BP are employed as an intermediate step between the CR3BP periodic solutions and the trajectories in the higher-fidelity ephemeris model. First, analogs of the 3:1 NRHO are constructed in the ephemeris force model for various epochs; the boundedness of the trajectories is measured using the apse angle mean values and standard deviations. The quality of the epoch prediction from the BCR4BP is explored. Second, the effects of the lower-fidelity model selected as the source of the initial guess for the transition are investigated. That is, the geometries of the 3:1 analogs in the ephemeris model are compared to the models used to generate the patch points. The speed of convergence, i.e., the number of iterations required for the differential corrections scheme to converge, are also compared.

A. 3:1 Analogs in the Ephemeris Model Employing the BCR4BP for the Initial Guess

Analogs for the Earth-Moon 3:1 NRHO are constructed in the Earth-Moon-Sun-Jupiter ephemeris model using the periodic 3:1 BCR4BP NRHO as the initial guess. Previously, the solutions in Figs. 7 and 9 leverage the 3:1 NRHO from the Earth-Moon CR3BP initial guess; for certain epochs, the resulting trajectories resemble the periodic orbit in the BCR4BP. Recall that the period of the 3:1 NRHO in the BCR4BP is precisely one synodic month, or equivalently, three orbital periods of the 3:1 NRHO in the CR3BP. Thus, to produce an initial guess for a 3-month trajectory in the ephemeris model, three revolutions of the 3:1 NRHO as computed in the BCR4BP are stacked. The trajectory is discretized with patch points placed approximately two days apart, then corrected for continuity in the Earth-Moon-Sun-Jupiter ephemeris model using a differential corrections scheme. The epoch corresponding to the first patch point is varied throughout the month of May 2023. The apse angles associated with each constructed trajectory are plotted in Fig. 10(a). Each line corresponds to the mean apse angle value of one lobe. For instance, the dark grey line in Fig. 10(a) corresponds to the mean apse angle value for the right (R) lobe. Additionally, the vertical error bars represent the standard deviation, $\pm\sigma_{\alpha,i}$, of the apse angle values at each epoch. Thus, the location (the mean value of the apse angles) and the spread (standard deviation of the apse angle) for each of the lobes in the bounded motions constructed for the month of May 2023 are summarized in Fig. 10(a). The apse angle values from the BCR4BP solution, $\bar{\alpha}_{i,4}$,are plotted as the dashed black lines for reference. Recall the definition of 'tightly converged' bounded motion within the context of this investigation: apolunes evenly distributed in three groups ($|\bar{\alpha}_L| \approx |\bar{\alpha}_R|$ and $\bar{\alpha}_C \approx 0$) and limited spread among the lobes ($\sigma_{\alpha,L}, \sigma_{\alpha,C}, \sigma_{\alpha,R} \leq 3^\circ$). Thus, initial epochs yielding tightly converged bounded motions in the ephemeris model are identified in Fig. 10(a) as the points where: (i) the gray lines approach the dashed lines, i.e., $\bar{\alpha}_i \approx \bar{\alpha}_{i,4}$ and (ii) the vertical lines are small, i.e., $\sigma_{\alpha,L}, \sigma_{\alpha,C}, \sigma_{\alpha,R} \approx 0$. A clear pattern appears in Fig. 10(a). Throughout the month of May 2023, there is an alternation of epochs that yield 'tightly converged' solutions and epochs that yield 'loosely converged' bounded motions. Three tightly converged solutions corresponding to the epoch indicated by the blue arrows and boxes in Fig. 10(a) are plotted in Figs. 10(b)–10(d). The initial epochs associated with these trajectories are approximately 9 days apart. The selected trajectories closely overlay the periodic orbit from the BCR4BP, denoted by the dashed black curve in Figs. 10(b)–10(d). Furthermore, recall that the 3:1 NRHO in the time-dependent BCR4BP is defined at two specific Earth-Moon-Sun configurations, summarized in Fig. 8 and Table 2. This information about epoch is not explicitly included in the initial guess for the ephemeris bounded motion; the epoch associated with the first patch point is varied between May 1st and May 30th, 2023. However, certain epochs during this time interval match the relative configuration of the Earth, Moon, and Sun that is predicted in the BCR4BP. Such epochs are denoted by the red vertical lines in Fig. 10(a). Note that these epochs correspond to the BCR4BP 3:1 NRHO in configuration 1 (see Fig. 8 and Table 2), which is the orbit employed for the initial guess. The epoch predictions approximately correspond to the epochs that result in tightly converged motions in the ephemeris model. Conversely, the epochs far from the BCR4BP predicted epochs yield more loosely converged solutions. Employing the 3:1 NRHO as computed in the BCR4BP as an initial guess for the transition to the ephemeris force model yields tightly converged bounded motions around the epochs predicted in the BCR4BP.

The repetition between tightly and loosely converged bounded motion in the ephemeris model is explored further. A zoomed view of Fig. 10(a) between May 20th and 30th, 2023, is presented in Fig. 11. The evolution of the geometry is apparent in this plot; loosely converged orbits are obtained at the beginning and end over this range of epochs. In the middle, the subset of epochs that yield tightly converged analogs is highlighted by the green dashed box. Note that with the boundedness criteria employed in this investigation, tightly converged solutions are constructed over a range of multiple days. The epoch prediction from the BCR4BP lies within the green box denoting the tightly converged analogs. Selected trajectories, denoted by the colored arrows in Fig. 11(a) are plotted in the Earth-Moon rotating frame; one is a tightly converged bounded motion, in Fig. 11(c), while the other two are at each end of the range of loosely converged

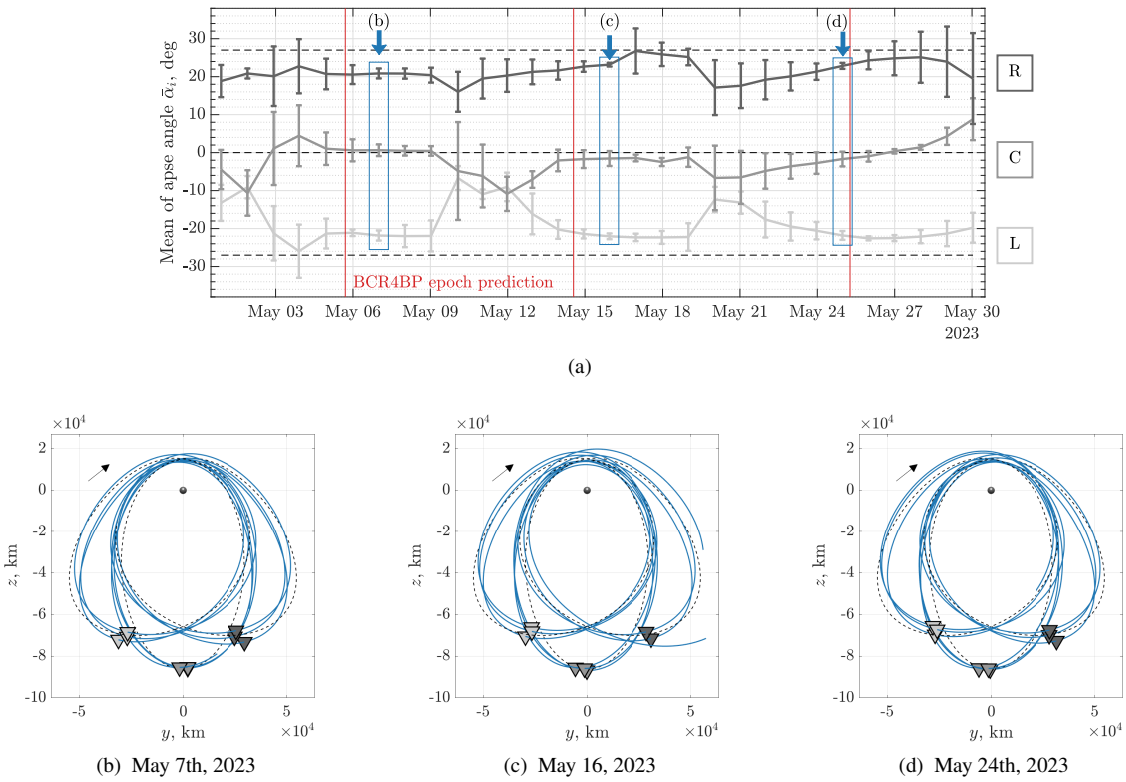

Fig. 10 Apse angles evolution as a function of the initial epoch for 9-revolutions of the 3:1 analogs in the Earth-Moon-Sun-Jupiter ephemeris for the month of May 2023 (a). The vertical error bars denote the $\pm\sigma_{\alpha,i}$ standard deviation. Trajectories for selected initial epochs as viewed in the Earth-Moon rotating frame (b,c,d), with the BCR4BP periodic orbit plotted as the dashed black line for reference.

trajectories, in Figs. 11(b) and 11(d). Note that the trajectories in Figs. 11(b) and 11(d) seem to mirror each other. While they are loosely converged solutions, three (unevenly distributed) groups of lobes are apparent in Figs. 11(b) and 11(d). For the trajectory originating on May 20th, 2023, the right lobes are pulled toward the positive Earth-Moon rotating $\hat{y}$ direction, in the direction of the black arrow in Fig. 11(b). Conversely, the left lobes along the trajectory in Fig. 11(d) are shifted towards the negative Earth-Moon rotating $\hat{y}$ direction. Thus, these 'loosely converged' trajectories are not phased correctly in terms of the relative positions of the Sun, Earth, and Moon, and the uneven gravitational action of the Sun is apparent.

While the 3:1 NRHO in the BCR4BP generally provides a favorable initial guess for both the geometry and the epoch for a bounded solution in the ephemeris model, further refinements of the initial guess may be required in certain cases. For instance, consider the 3:1 analogs computed in the Earth-Moon-Sun-Jupiter ephemeris model for the month of July 2026 in Fig. 12(a). Similar to Fig. 10(a), the pattern of tightly and loosely converged epochs is observed throughout the month. Favorable Sun-Earth-Moon orientations predicted by the BCR4BP are indicated by vertical red lines. Three solutions constructed in the ephemeris model are plotted in the Earth-Moon rotating frame in Figs. 12(b)–12(d); these trajectories correspond to the epochs designated by the colored arrows and boxes in Fig. 12. The blue trajectory, in Fig. 12(b), appears reasonably well-aligned, i.e., it corresponds to the minimum standard deviation for the apse angles, within a few days of the epoch predicted by the BCR4BP. The other two trajectories, in Figs. 12(c) and 12(d), are selected with initial epochs on either side of the epoch predicted by the BCR4BP. Note that these two trajectories do not satisfy the conditions for tight convergence: the standard deviations associated with one or multiple lobes is greater than 3°. While the solution in Fig. 12(c) may be acceptable for certain applications, the three-lobe geometry visibly breaks down for the trajectory in Fig. 12(d). Therefore, while the geometry from the BCR4BP periodic orbit still exists in the higher-fidelity ephemeris model, it is not maintained at the specific epoch predicted by the lower-fidelity model.

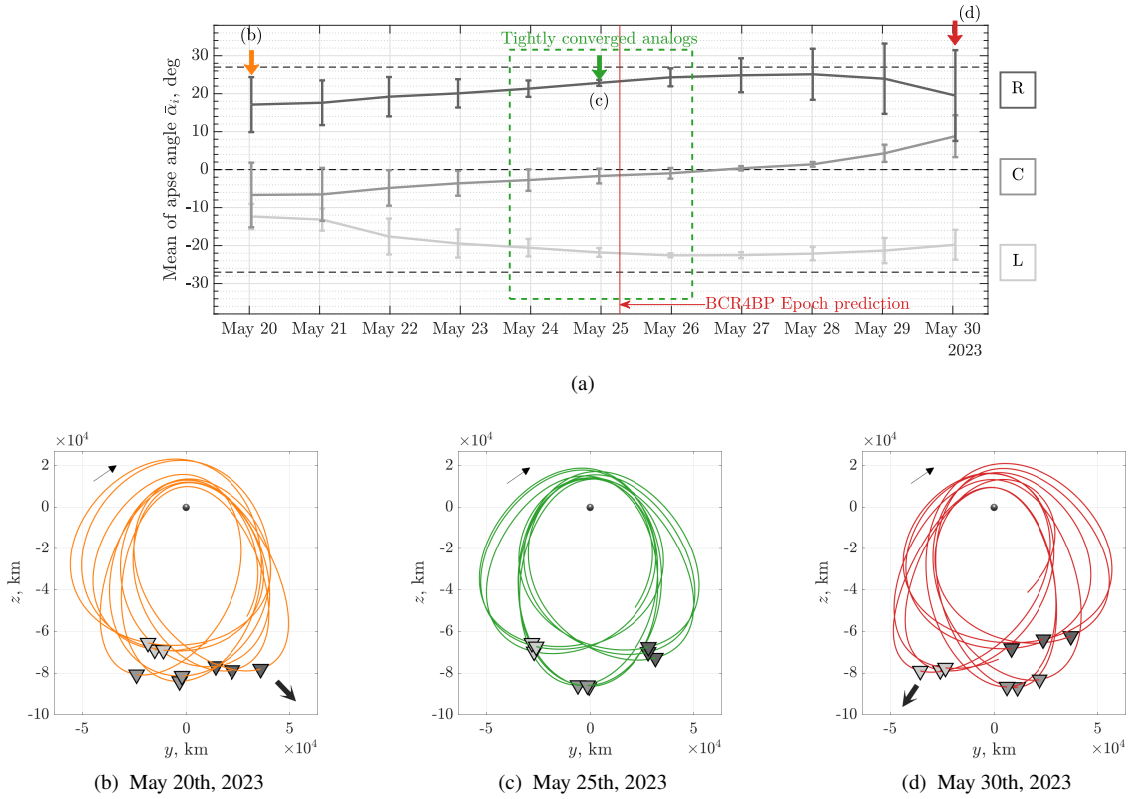

Fig. 11 Zoomed view of Fig. 10(a) between May 20th and May 30th, 2023 (a). The vertical error bars denotes the $\pm\sigma_{\alpha,i}$ standard deviation. The subset of initial epoch yielding tightly converged analogs is boxed in green. Trajectories for select initial epochs as viewed in the Earth-Moon rotating frame (b,c,d).

Additional perturbations that are included in the higher-fidelity model may be one explanation for this discrepancy. Recall that the Earth, Moon, and Sun are assumed to be in circular, coplanar orbits in the BCR4BP. Consequently, the inclination of the lunar orbit with respect to the ecliptic plane and, perhaps significantly, the eccentricity of the lunar orbit are not included in the BCR4BP, but are actively perturbing the bounded motion in the ephemeris model. Further investigation into the role that these perturbations play for the convergence of the 3:1 NRHO in the ephemeris force model is necessary. Although the BCR4BP provides a suitable initial guess for both the geometry and the epoch of tightly converged 3:1 analogs in the ephemeris model, additional perturbations that are not included in this lower-fidelity model may influence the convergence process at certain epochs.

B. Comparison Between CR3BP and BCR4BP for Initial Guess Generation

The effectiveness of the BCR4BP as an intermediate step to transition the 3:1 NRHO from the CR3BP to the ephemeris model is examined. The trajectories produced in Fig. 10 are compared to trajectories that do not employ the BCR4BP as an intermediate model, that is, trajectories that are directly transitioned from the Earth-Moon CR3BP. The geometries of the solutions are compared in Fig. 13. The plots on the left, Figs. 13(a), 13(c) and 13(e), represent the mean apse angle values for each group of lobes, i.e., the location of the lobes. The plots on the right, Figs. 13(b), 13(d) and 13(f), summarize the spread among each group of lobes, that is, the standard deviation for the apse values. Both solution sets are computed over the same range of epochs, May 1st through May 30th, and possess the same time-of-flight equal to 3 months. The solutions constructed using nine revolutions from the CR3BP 3:1 NRHO as the initial guess are plotted in red in Fig. 13, while trajectories initialized with three revolutions of the BCR4BP counterpart of the 3:1 NRHO are plotted in blue. First, note that employing the BCR4BP as an intermediate step yields the three-lobe geometry throughout the month more consistently than solely relying on the CR3BP for the initial guess. In Figs. 13(a), 13(c) and 13(e), the blue lines are generally closer than the red lines to the reference apse angle values from the BCR4BP,

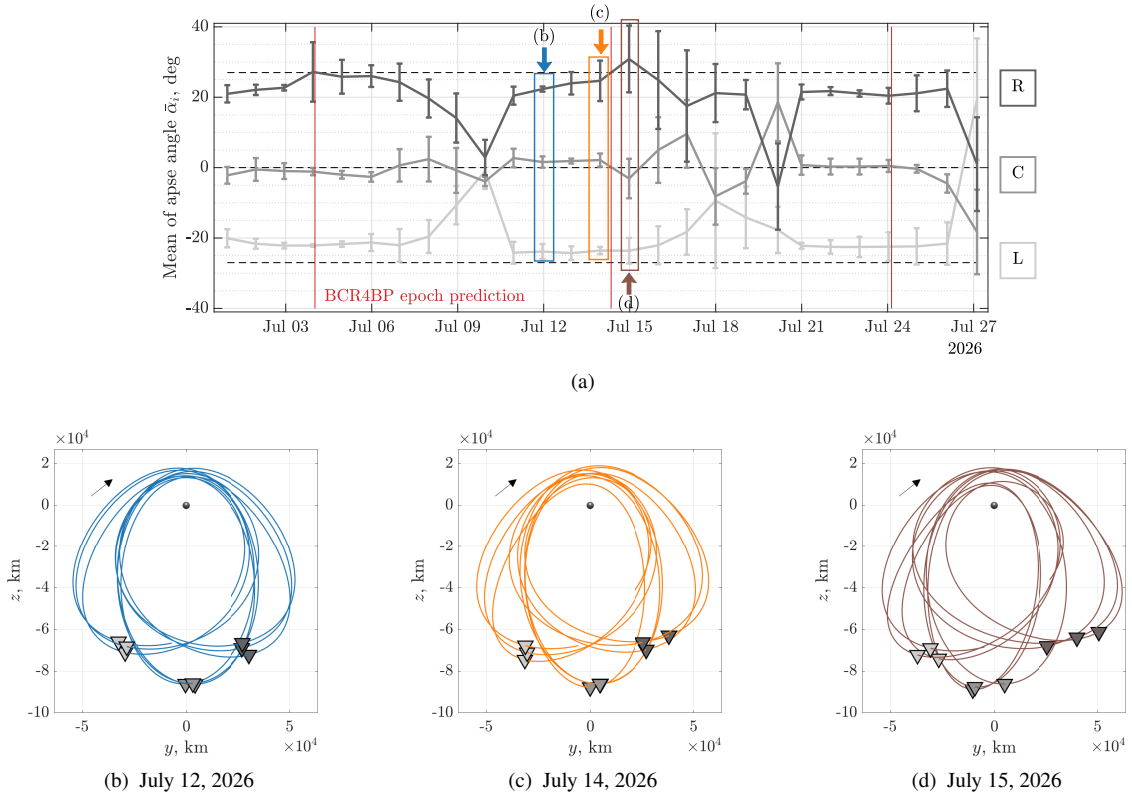

(b) July 12, 2026 (c) July 14, 2026 (d) July 15, 2026

Fig. 12 Apse angles evolution as a function of the initial epoch for 9-revolutions 3:1 analogs in the Earth-Moon-Sun-Jupiter ephemeris for the month of July 2020 (a). The vertical error bars denotes the $\pm\sigma_{\alpha,i}$ standard deviation. Trajectories for select initial epochs as viewed in the Earth-Moon rotating frame: trajectory with the minimum apse angle standard deviation (b) and trajectories around the epoch predicted by the BCR4BP (c,d).

represented by the black dashed lines. Additionally, the variations in the apse locations are generally larger for the solutions employing the CR3BP solution as the initial guess, apparent from the large variations of the red curve in Figs. 13(a), 13(c) and 13(e). Second, employing the BCR4BP solutions as an intermediate step in the transition to the ephemeris model results in less spread among each group of lobes, as presented in Figs. 13(b), 13(d) and 13(f). The standard deviation in the apse angles along the ephemeris solution is generally between 1° and 10° when using the BCR4BP intermediate step, while it ranges between 5° and 15° for most epochs when directly transitioning a CR3BP periodic orbit. Thus, employing the BCR4BP periodic orbit as an initial guess generally results in bounded motions with tighter geometries in the ephemeris model. Finally, note that the ranges of epochs that yields tightly converged solutions is comparable for the two solution sets. The dark arrows in Fig. 13 indicate the epochs corresponding to tight geometry in Figs. 10(b)–10(d). For these epochs, the locations of each group of lobes is similar between the two solution sets, as apparent in Figs. 13(a), 13(c) and 13(e). However, from Figs. 13(b), 13(d) and 13(f), the trajectories in the ephemeris model generated from the BCR4BP periodic orbit tend to deliver less dispersion in each group of lobes. While the direct transition from the CR3BP to the ephemeris yields a 'tightly converged' solution in the ephemeris model at certain epochs, employing the BCR4BP as an intermediate step generally improves the characteristics of the geometry in the resulting trajectories over the majority of epochs.

The convergence rates of the two transition methods, that is, the direct transition from the CR3BP and the method employing the BCR4BP as an intermediate step, are also compared. Within the context of this investigation, the convergence rate is defined as the required number of iterations for the constraints in the differential corrections scheme to achieve a specified tolerance. For a meaningful comparison, the corrections scheme is identically formulated for both transition methods. The time-of-flight associated with each initial guess is the same (3 months), the discretization of each trajectory is identical (patch points are placed every two days), and the same constraints are enforced (continuity

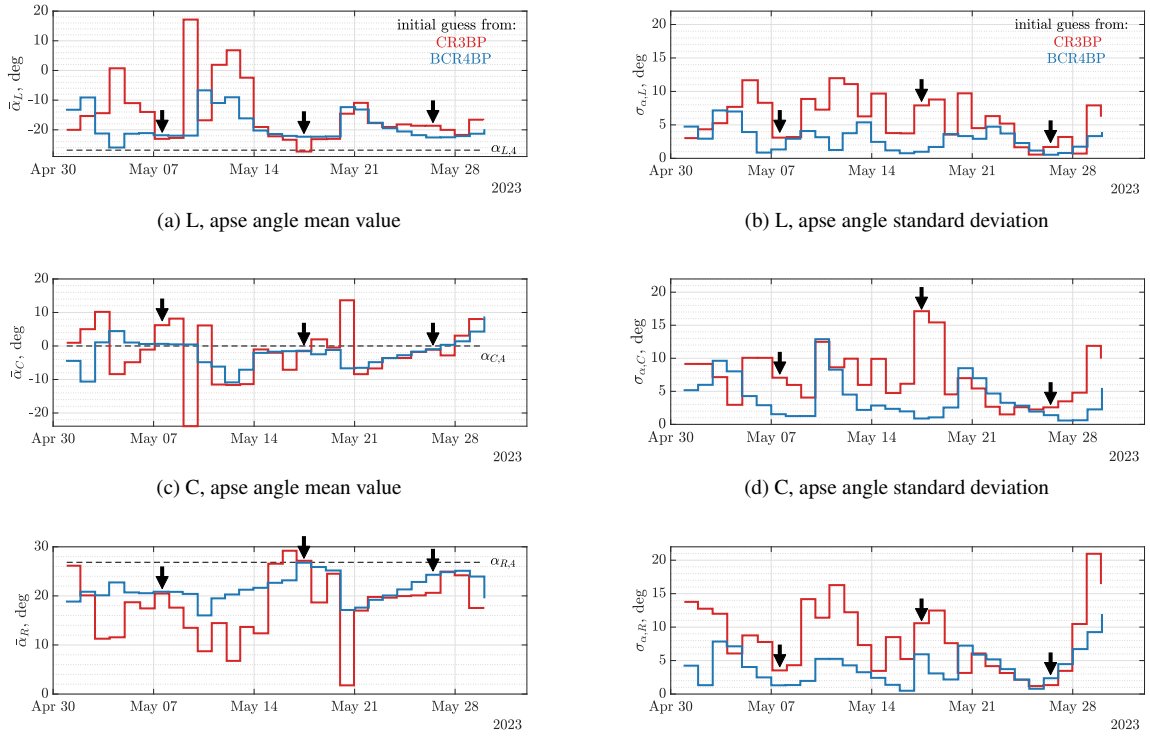

(a) L, apse angle mean value

(b) L, apse angle standard deviation

(c) C, apse angle mean value

(d) C, apse angle standard deviation

(e) R, apse angle mean value

(f) R, apse angle standard deviation

Fig. 13 Comparison of the geometries of 3:1 NRHOs computed in the ephemeris model for the month of May 2023 using patch points from the CR3BP (red) or the BCR4BP (blue) as an initial guess. The black arrows indicate the tightly converged solutions plotted in Figs. 10(b)–10(d).

constraints between consecutive arcs). The differences between the approaches reside in the location, in position and velocity spaces, of the patch points themselves. Since a different lower-fidelity model is employed in each transition method, a different set of initial patch points, plotted in Fig. 14(b), is employed to commence the corrections process. The number of iterations required to produce the bounded solutions in Fig. 13, i.e., those that satisfy the constraints to a specified tolerance, is plotted as a function of the initial epoch in Fig. 14(a). Employing the BCR4BP periodic orbit as the initial guess generally results in a faster convergence, i.e., a lower number of iterations for the corrections scheme. The direct transition from the CR3BP converges on average in 16 iterations, as opposed to 11 iterations on average for the method employing the BCR4BP as an intermediate step. Additionally, note the link between the number of iterations and geometry of the resulting trajectory in the ephemeris model. Tightly converged solutions, highlighted by the black arrows in Fig. 14(a), require fewer iterations than the loosely converged solutions. The strategy incorporating the BCR4BP for the initial guess, in particular, requires 10 iterations or fewer to converge for these solutions. Employing the BCR4BP as an intermediate step for the computation of the analogs of the 3:1 NRHO in the ephemeris model noticeably increases the convergence rate for the differential corrections scheme.

VI. Concluding Remarks

Stacking revolutions of a periodic orbit in a lower-fidelity model and employing a differential corrections scheme is an effective strategy to construct bounded motion or quasi-periodic orbits in the ephemeris model and produces useful analogs that preserve the characteristics that are deemed important for the application. A direct transition from the lower- to the higher-fidelity model is sufficient in many cases to maintain the desired characteristics and geometry of the solution throughout the transition. However, the transition is not smooth and the analogs do not meet the desirable criteria for certain periodic orbits from the Earth-Moon CR3BP, such as the L_2 3:1 synodic resonant NRHO. When directly transitioned from the CR3BP, the resulting solution in the ephemeris model results in either a ‘tightly’ or

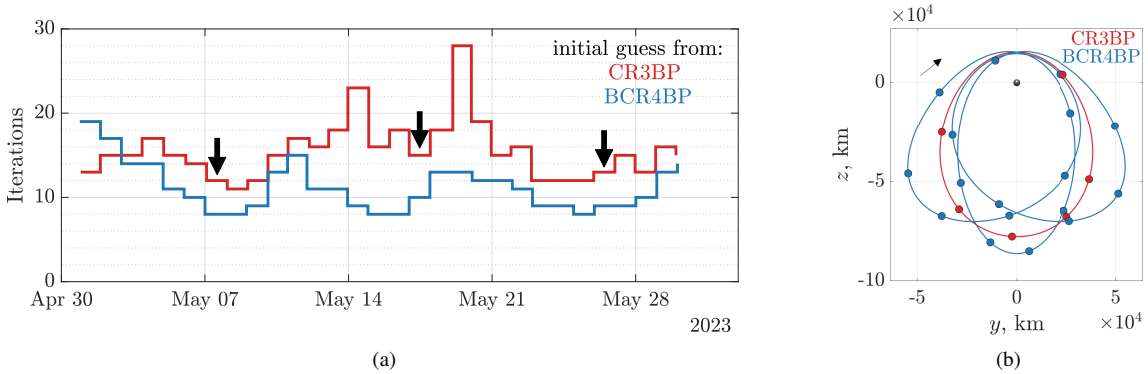

Fig. 14 Comparison of the number iterations required in the differential corrections scheme for the trajectories in Fig. 13, using patch points from the CR3BP (red) or the BCR4BP (blue) as an initial guess (a). The black arrows indicate the tightly converged solutions plotted in Figs. 10(b)–10(d). Patch point placement as viewed in the Earth-Moon rotating frame (b).

'loosely' converged geometry; neither type of solution resembles the periodic orbit in the CR3BP. While the orbital and stability characteristics of the 3:1 NRHO in the CR3BP do not set it apart from the other orbits in the L_2 halo family of periodic orbits, it does exist in a complex dynamical environment. Multiple bifurcations to other families of periodic orbits exist in the near vicinity of the 3:1 NRHO. Transitioning the 3:1 NRHO directly from the CR3BP to the ephemeris model is not an effective way to construct bounded, repeatable motion in the higher-fidelity model.

Solutions in the ephemeris model that present the 'tightly' converged geometry resemble the three-lobe geometry of the 3:1 NRHO as computed in the Earth-Moon-Sun BCR4BP, although these solutions are constructed employing the periodic orbit from the Earth-Moon CR3BP as the initial guess. Therefore, this investigation proposes a transition method to the ephemeris model that employs the periodic orbit in the BCR4BP as an intermediate step. Since the BCR4BP is a periodic, time-dependent model, the analog of the 3:1 synodic resonant NRHO exists at specific configurations of the Earth, Moon, and Sun. A method is proposed to convert the BCR4BP epoch parameter, that is, the Sun angle, to an epoch that is employed in the ephemeris model. Additionally, metrics are proposed to describe the boundedness of an analog of the 3:1 NRHO in the ephemeris force model. The apse angle describes the location of a lobe of the 3:1 NRHO, when represented in the Earth-Moon rotating frame. For a multi-revolution solution, the location of each group of lobes is described by the mean value of the apse angles, while the 'spread' of the lobes is quantified by the standard deviation of the apse angles. In the ephemeris model, 'tightly converged' solutions that resemble the 3:1 NRHO from the BCR4BP possess three evenly distributed groups of lobes that present limited spread.

Employing the BCR4BP as an intermediate step in the transition process is an effective way to construct the analogs of the 3:1 NRHO with bounded, repeatable motion in the ephemeris force model. Tightly converged trajectories are generated in the Earth-Moon-Sun-Jupiter ephemeris model for a variety of initial epochs. Additionally, the BCR4BP generally accurately predicts the ranges of initial epochs that yield tightly converged solution in the higher-fidelity model. For solutions beyond these ranges of initial epochs, the uneven gravitational influence of the Sun on the geometry is apparent. However, additional perturbations that are not included in the BCR4BP or in the CR3BP, such as the effects of the eccentricity of the lunar orbit, may have a non-negligible influence on the transition process at certain epochs. Further investigation into the role that these perturbations play for the convergence of the 3:1 NRHO in the ephemeris force model is necessary. The effectiveness of the BCR4BP as an intermediate step to transition the 3:1 NRHO from the CR3BP to the ephemeris model is verified. Across a range of initial epochs, the analogs of the 3:1 NRHO constructed in the ephemeris model employing the BCR4BP periodic orbit as the initial guess generally retain the three-lobe geometry better than the solutions that are directly transitioned from the CR3BP. Additionally, for the same transition scenario, the corrections schemes tend to converge in a lower number of iterations when employing the 3:1 NRHO from the BCR4BP as the initial guess. The transition of the Earth-Moon 3:1 synodic resonant NRHO to the ephemeris force model is facilitated when an intermediate model, the Earth-Moon-Sun BCR4BP, is leveraged.

Acknowledgments

This work was conducted at Purdue University and NASA Johnson Space Center under contract number NNJ13HA01C with additional effort under cooperative agreement NNX13AK60A and grant #80NSSC18M0122. This research was also supported by a Purdue Bilsland Dissertation Fellowship. The authors thank Beom Park at Purdue University and Emily Zimovan-Spreen at Johnson Space Center for useful discussions. Also acknowledged is the Purdue University School of Aeronautics and Astronautics for facilities and support, including access to the Rune and Barbara Eliasen Visualization Laboratory.

References

[1] International Space Exploration Coordination Group, *The Global Exploration Roadmap*, NASA, 2018.

[2] Lee, D. E., "White Paper: Gateway Destination Orbit Model: A Continuous 15 Year NRHO Reference Trajectory," Tech. rep., NASA, 2019.

[3] Szebehely, V. G., *Theory of Orbits, the Restricted Problem of Three Bodies*, Academic Press, 1967.

[4] Huang, S.-S., *Very Restricted Four-Body Problem*, NASA technical note, National Aeronautics and Space Administration, 1960.

[5] Gómez, G., Llibre, J., Martínez, R., and Simó, C., *Dynamics And Mission Design Near Libration Points - Vol II: Fundamentals: The Case Of Triangular Libration Points*, World Scientific Monograph Series In Mathematics, World Scientific Publishing Company, 2001. https://doi.org/10.1142/4402.

[6] Jorba-Cuscó, M., Farrés, A., and Jorba, A., "Two Periodic Models for the Earth-Moon System," *Frontiers in Applied Mathematics and Statistics*, Vol. 4, 2018, p. 32.

[7] Boudad, K. K., "Disposal Dynamics From The Vicinity Of Near Rectilinear Halo Orbits In The Earth-Moon-Sun System," M.S. Thesis, Purdue University, West Lafayette, Indiana, 2018.

[8] Jet Propulsion Laboratory, "SPICE Toolkit," https://naif.jpl.nasa.gov/naif/aboutspice.html, 2000.

[9] Zimovan, E. M., Howell, K. C., and Davis, D. C., "Near Rectilinear Halo Orbits and their Application in Cis-Lunar Space," *3rd International Academy of Astronautics Conference on Dynamics and Control of Space Systems*, Moscow, Russia, 2017.

[10] Zimovan-Spreen, E. M., Howell, K. C., and Davis, D. C., "Near Rectilinear Halo Orbits and Nearby Higher-Period Dynamical Structures: Orbital Stability and Resonance Properties," *Celestial Mechanics and Dynamical Astronomy*, 2020.

[11] Broucke, R. A., "Stability of Periodic Orbits in the Elliptic, Restricted Three-Body Problem," *AIAA Journal*, 1969. https://doi.org/10.2514/3.5267.

[12] Boudad, K. K., Howell, K. C., and Davis, D. C., "Dynamics of Synodic Resonant Near Rectilinear Halo Orbits in the Bicircular Four-Body Problem," *Advances in Space Research*, Vol. 66, No. 9, 2020, pp. 2194–2214. https://doi.org/https://doi.org/10.1016/j.asr.2020.07.044.

[13] Boudad, K. K., Davis, D. C., and Howell, K. C., "Near Rectilinear Halo Orbits in Cislunar Space within the Context of the Bicircular Four-Body Problem," *2nd IAA/AAS SciTech Forum*, Moscow, Russia, 2019.

[14] Pritchett, R., "Strategies For Low-Thrust Transfer Design Based on Direct Collocation Techniques," Ph.D. thesis, Purdue University, West Lafayette, Indiana, 2020.

[15] Vutukuri, S., "Spacecraft Trajectory Design Techniques Using Resonant Orbits," M.S. Thesis, Purdue University, West Lafayette, Indiana, 2018.

[16] Meyer, K., and Hall, G., *Introduction to Hamiltonian Dynamical Systems and the N-Body Problem*, Applied Mathematical Sciences, Springer New York, 2013.

[17] Yakubovich, V., and Starzhinskii, V., *Linear Differential Equations with Periodic Coeffcients*, Vol. 1, John Wiley and Sons, New York, 1975.

[18] Davis, D. C., Boudad, K. K., Power, R. J., Howell, K. C., and Sweeney, D. J., "Heliocentric Escape and Lunar Impact from Near Rectilinear Halo Orbits," *AAS/AIAA Astrodynamics Specialist Conference*, Portland, Maine, 2019.

[19] Campbell, E., "Bifurcations from Families of Periodic Solutions in the Circular Restricted Problem with Applications to Trajectory Design," Ph.D. thesis, Purdue University, West Lafayette, Indiana, 1999.

[20] Hale, J., Buttanri, H., and Kocak, H., *Dynamics and Bifurcations*, Texts in Applied Mathematics, Springer New York, 1996.

[21] Seydel, R., *Practical Bifurcation and Stability Analysis*, Interdisciplinary Applied Mathematics, Springer New York, 2009.

[22] Zimovan-Spreen, E., "Trajectory Design and Targeting for Applications to the Exploration Program in Cislunar Space," Ph.D. Dissertation, Purdue University, West Lafayette, Indiana, 2021.

[23] Davis, D. C., Phillips, S. M., Howell, K. C., Vutukuri, S., and McCarthy, B. P., "Stationkeeping and Transfer Trajectory Design for Spacecraft in Cislunar Space," *AAS/AIAA Astrodynamics Specialist Conference*, Columbia River Gorge, Stevenson, Washington, 2017.

[24] Espenak, F., and Dutta, S., "SKYCAL (Sky Events Calendar)," https://eclipse.gsfc.nasa.gov/SKYCAL/SKYCAL.html, 2007. NASA GSFC.

[25] Guzzetti, D., Zimovan, E. M., Howell, K. C., and Davis, D. C., "Stationkeeping analysis for spacecraft in lunar near rectilinear halo orbits," *Advances in the Astronautical Sciences*, 2017.